Biocompatible polythiophene-*g*-polycaprolactone copolymer as efficient dopamine sensor platform

Brenda G. Molina,[1,2] Anca D. Bendrea,[3] Luminita Cianga,[3] Elaine Armelin,[1,2,*] Luis J. del Valle,[1,2] Ioan Cianga,[3,*] and Carlos Alemán[1,2,*]

[1] Maristany, 10-14, Ed. I2, 08019, Barcelona, Spain

[2] Catalunya, C/ Eduard Maristany, 10-14, Ed. C, 08019, Barcelona, Spain

[3] Ghica Voda Alley, 700487, Iasi, Romania

Correspondence to: elaine.armelin@upc.edu, ioanc@icmpp.ro and carlos.aleman@upc.edu

ABSTRACT

Amphiphilic copolymers consisting of an all conjugated polythiophene backbone and sparsely attached oligo- -caprolactone side chains have been prepared by anodic electropolymerization of hydroxymethyl-3,4-ethylenedioxythiophene (HMeEDOT) with a thiophene-ended oligo- -caprolactone macromonomer (Th-PCL), obtained by ring opening polymerization of -caprolactone with thiophene methanol. The random copolymers, obtained starting from two different molar ratios of the co-monomers in the feed (HMeEDOT : Th-PCL of 80:20 and 60:40), and the homopolymer (PHMeEDOT) were synthesized by using three different working electrodes. After structural characterization by FTIR, the electrochemical, morphological and surface properties of the obtained copolymers were examined, results evidencing a dependence on both the working electrode and the composition in the feed. In order to evaluate the opportunity of copolymers's further bioapplications, biodegradability, cytotoxicity and cell proliferation investigations were carried out. By combining the results of electrochemical characterization with those of biocompatibility and dopamine sensing capability, it was concluded that co-monomers feed ratio of 80:20 could be the optimal choice for the potential use of these amphiphilic copolymers in sensing devices. All in all, this study shows the benefit of a designed "hairy-rod" conjugated polymeric architecture which, *via* the side chains nature (biocompatible / biodegradable, hydrophobic, oligomeric) and their grafting density, enabled the synthesis of a material for targeted application.

INTRODUCTION

The synthesis of hybrid organic materials composed of a bio-based polymer and a synthetic polymer (natural-synthetic hybrids) or two synthetic polymers with very different chemical characteristics and properties (synthetic-synthetic hybrids) is gaining interest for a variety of biomedical applications.[1-5] These hybrids are usually structured as block[6-8] or graft[9-13] copolymers.

Conjugated conducting polymers (CPs), one of the most fascinating examples of specialty soft materials, have undergone an unprecedented pace of development in the last four decades. Their shape persistence and intrinsic ability to self-assembly make them distinguishable,[14] while these features bring them closer to biomolecules.[15] CPs possess very good electrical and optical properties, have a high conductivity/weight ratio and can be non-cytotoxic.[16-21] Furthermore, a great advantage of CPs is that their properties can be tailored to the specific needs of their applications by incorporating other compounds.[22-25]

On the other hand, *"Hairy-rod"* CPs (HR-CPs), far from being a fancy name, emerged as an important concept stated by Wegner, which defined them as "molecular composites" in order to underline their hybrid nature and, moreover, that their components are dispersed at the molecular level.[15,26] By comparing with other topologies, HR-CPs' complexity is only partly attained by *"molecular brushes"*[27,28] [with which HR-CPs share the shape persistence motive and polymerization strategies.[29]

Wegner pointed out that HR-CPs are excellently suited to advance new concepts in the chemical, biomedical and electronics industry[15] and, the progress in macromolecular chemistry, noteworthy of controlled radical polymerization, allowed the obtainment of HR-CPs with well-defined oligomeric side chains attached on the main chain, resulting in copolymers of *rod-coil* type.[29-34] Inherent rod-like stiffness of the conjugated main chain, beside its fluorescence, electrical properties and - interaction capability as well as the structural stiff asymmetry between rod and coil counterparts determine HR-

rod-coil conjugated block copolymers (BCPs), although they have similar propensity for self-assembling, it seems that the morphology and the properties of HR-CPs are significantly better when used for electronic devices.[33] More freedom in tunability of morphology and physical properties by changing side chains nature and position,[29] grafting density and length,[34-40] in a controlled manner, represent another advantages by comparison with their linear BCPs analogs. Due to these advantages, HR-CPs were found to be appropriate materials for optoelectronic devices,[33,34,41,42] as well as for biomedical applications. For example, hybrid materials consisting of all conjugate polythiophene (PTh) backbone and well-defined poly(ethylene glycol) (PEG) grafted chains were prepared and successfully used as both active surfaces for the selective adsorption of proteins and substrates to promote the electrocommunication will cells.[35,37,39] The fluorescent HR-CPs, decorated with biocompatible and functional side chains, were investigated for cells imaging,[38,43,44] while construction of biosensors based on such polymers was reported as well.[45,46]

In this work we present the synthesis and characterization of new PTh-based graft copolymers with oligo- -caprolactone grafted chains. These materials combine the technological advantages of each component, allowing biofunctional applications. More specifically, poly(3,4-ethylenedioxythiophene) (PEDOT; Scheme 1) is a PTh derivative that, in addition of being successfully used in many electronic applications (*e.g.* supercapacitors, organic light-emitting diodes and solar cells),[47,48] has been proposed as a fundamental material for the selective detection of dopamine (DA).[49,50] The latter is an important neurotransmitter of catecholamine in

disease and Parkinson disease.[51] In a recent study we addressed a rational design approach oriented to enhance the binding affinity of PEDOT towards DA.[52] We found that sensors based on poly(hydroxymethyl-3,4-ethylenedioxythiophene) (PHMeEDOT; Scheme 1), which simply incorporates a hydroxymethyl substituent to the dioxane ring (Scheme 1), exhibit better sensitivity and selectivity for the determination of DA than PEDOT.

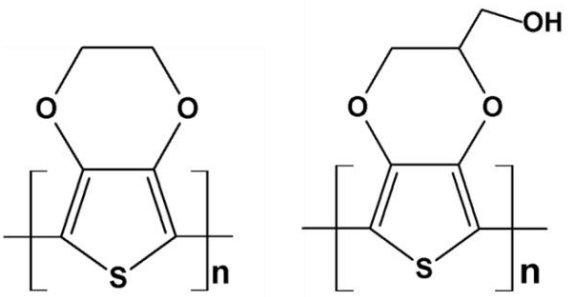

Scheme 1: PEDOT (left) and PHMeDOT (right).

Currently, an important handicap of DA sensing devices is that they are invasive, which severely restricts their implantation for continuous monitoring. In order to avoid this drawback, the biocompatibility of PTh-based CPs, including PEDOT and PHMeEDOT, needs to be enhanced improving the interactions between the synthetic material and the cells. The new biofunctional PTh-*g*-PCL copolymers obtained in this work avoid the drawback of traditional CP-based sensors. Thus, the remarkable biocompatibility of oligo- -caprolactone side chains is not interfering with the detection ability of the PTh backbone and *vice-versa*.

Although some CP-*g*-PCL copolymers are described in the literature,[31,53-57] those studies were mostly focused on their complex synthesis or on their films morphology investigation,[58,59], and only few of them have considered these type of copolymers potential applications.[43,44,60,61]

grafting through *macromonomer*

and electropolymerization technique for synthesis of new PTh-*g*-PCL copolymers. As electropolymerization is a kind of *"two in one"* technique, allowing concomitantly the polymerization as well as the thin film formation of polymers, it is very appropriate for stimuli sensitive, functional surface construction derived from HR-CPs and, as it was already noticed for such type of topology,[62] it is a valuable alternative to so-called *"polymer brushes"*,[63] that are prepared through more costly and technically difficult surface initiated polymerization.[64] Accordingly to previous assumptions, thiophene-ended oligo- -caprolactone macromonomer Th-PCL has been anodically polymerized with HMeEDOT as co-monomer in two different

molar ratio. After physicochemical characterization of the macromoner and copolymers, the cytotoxicity, biocompatibility and ability to detect DA have been investigated. The experimentally results successfully showed that the use of macromonomer not only improves the biocompatibility of resulting materials by reducing toxicity of PHMEDOT, but also enhance the sensitivity and selectivity of the PTh backbone for the detection of DA.

METHODS

Materials. 3-thiophene-methanol (Th-MeOH) (Aldrich), -caprolactone (-CL; Aldrich), stannous octanoate (Sigma), hydroxymethyl-3,4-ethylenedioxythiophene (HMeEDOT; Sigma-Aldrich, 95%) and acetonitrile (Panreac S.A., PA) were used as received. Tetrabutylammonium tetrafluoroborate (TBATFB; Sigma-Aldrich, 95%) was stored in an oven at 80 °C before its use in the electrochemical trials. The other used solvents were purified and dried by usual methods.

chloride and magnesium chloride, was prepared as electrolyte solution for electrochemical trials. DA hydrochloride (3-hydroxytyramine hydrochloride), ascorbic acid (AA; L-configuration, crystalline) and uric acid (UA; crystalline) of analytical reagent grade were purchased from Sigma-Aldrich (Spain).

For cell culture experiments, Cos-1 and Vero cells (kidney epithelial and fibroblast cells, respectively; obtained from African green monkey, *Cercopithecus aethiops*) were purchased

glucose/L, 110 mg of sodium pyruvate/L and (2 mM) L-glutamine), penicillin-streptomycin, 3-(4,5-dimethylthiazol-2-yl)-2,5-diphenyltetrazolium bromide (MTT, 97.5%) and trypsin-EDTA solution (0.05% trypsin, 0.02% EDTA) were all purchased from Sigma-Aldrich (USA). Fetal bovine serum (FBS) and trypan blue stain (0.4%) were purchased from Gibco, UK. Dimethyl sulfoxide (99.0%) was purchased from Panreac Quimica S.A.U. (Spain) and sodium azide

-Aldrich (USA).

Characterization of the macromonomer. ^{1}H-NMR spectra were recorded at room temperature on a Bruker Avance DRX-400 spectrometer (400 MHz) as solutions in acetone-d_6 and $CDCl_3$. Chemical shifts are reported in ppm and referenced to TMS as internal standard.

DSC experiments were performed on a Perkin Elmer DSC-6 differential scanning calorimeter, in the range of 10 120ºC, under nitrogen at a scanning rate of 10 ºC/min.

The weight fraction crystallinity ($_c$) was evaluated using Eq 1,[65]

$$_c \quad \frac{H_m}{H_m^0} \; 100 \qquad (1)$$

where H_m is the measured melting enthalpy and H_m^0 is the enthalpy of melting of the 100% crystalline PCL, with value of 139 J/g.[66]

FTIR spectra were recorded on a Bruker Vertex 70 FTIR spectrometer equipped with a diamond ATR device (Golden Gate, Bruker) in transmission mode, by using KBr pellets.

Polymerization. The homopolymer and the copolymers were prepared by chronoamperometry (CA) with an Autolab PGSTAT302N equipped with the ECD module (Ecochimie, The Netherlands) using a three-electrode cell under a nitrogen atmosphere (99.995% in purity) at room temperature. Steel AISI 316L and ITO sheets of 0.5 0.5 cm^2 area were employed as working electrode for characterization studies, while glass carbon (GC) electrodes of 2 mm diameter were used for detection assays. The counter electrode was made of AISI 316L while the reference electrode was an Ag|AgCl electrode containing a KCl saturated aqueous solution (E^0 = 0.222 V at 25ºC), which was connected to the working compartment through a salt bridge containing the electrolyte solution.

For preparation of PHMeEDOT, the anodic compartment was filled with 5 mL of a 10 mM acetonitrile solution of HMeEDOT containing 0.1 M TBATFB as supporting electrolyte, while the cathodic compartment was filled with 10 mL of the same electrolytic solution. Polymerizations were carried out applying a constant potential of +1.50 V during a generation time ( ) of 500 seconds. On the other hand, PTh-*g*-PCL copolymers were prepared considering

80:20 and 60:40 HMeEDOT:Th-PCL molar ratios at the same total molar concentration in solution. Copolymers were also obtained applying a potential of +1.50 V, whereas the polymerization time was adjusted as a function of the monomers ratio: = 500 and 800 s for 80:20 and 60:40 HMeEDOT:Th-PCL ratios, respectively.

Characterization of the prepared polymers. FTIR spectra of PHMeEDOT, its corresponding monomer and both 80:20 and 60:40 PTh-*g*-PCL copolymers were recorded on a Nicolet 6700 spectrophotometer equipped with a transmission accessory and using KBr pellets. The samples were evaluated using OMNIC software at 64 scans between 4000 and 500 cm^{-1} and resolution of 2 cm^{-1}.

The surface morphology was examined using scanning electron microscopy (SEM). Dried samples were placed in a Focused Ion Beam Zeiss Neon 40 scanning electron microscope operating at 5 kV, equipped with an EDX spectroscopy system.

UV-vis spectra were carried out in a UV-vis-NIR Shimadzu 3600 spectrophotometer equipped with a tungsten halogen visible source, a deuterium arc UV source, a photomultiplier tube UV-vis detector, and a InGaAs photodiode and cooled PbS photocell NIR detectors. Samples were deposited onto ITO substrate. Spectra were recorded in the absorbance mode using the integrating sphere accessory (model ISR-3100), the range wavelength being 350-750 nm. The interior of the integrating sphere was coated with a highly diffuse BaSO4 reflectance standard. Single-scan spectra were recorded at a scan speed of 60 $nm \cdot min^{-1}$. Measurements, data collection and data evaluation were controlled by the computer software UVProbe version 2.31.

Electrochemical characterization was carried out by cyclic voltammetry (CV) using the above mentioned Autolab PGSTAT302N. Experiments were conducted in a phosphate buffer solution (PBS) 0.1 M (pH= 7.4) at room temperature. The initial and final potentials were 0.4 V, and the reversal potential was +0.8 V. A scan rate of 50 mV/s was used. The ability to exchange charge reversibly (*i.e.* electroactivity) and the electrochemical stability (*i.e.* electrostability) were determined through direct measure of the anodic and cathodic areas in the

control voltammograms using NOVA software. The loss of electroactivity (LEA, in %) was expressed as:

$$LEA \quad \frac{\Delta Q}{Q_I} \cdot 100 \qquad (1)$$

cycle,

and Q_I is the voltammetric charge corresponding to the first cycle.

Contact angle ( ) measurements were carried out with the water sessile drop method. Images of MilliQ water drops (0.5 L) were recorded after stabilization with an OCA 15EC instrument (Data-Physics Instruments GmbH, Filderstadt). SCA20 software was used to analyze the images and determine the u value, which was obtained as the average of at least eight independent measures for each sample.

Film thickness measurements were carried out using a Dektak 150 stylus profilometer (Veeco, Plainview, NY).

Degradation. Degradation studies were carried for polymeric films deposited on steel electrodes. Films were placed in PBS (pH= 7.4) and incubated at 37 ºC in a shaking incubator at 100 rpm for a total of five weeks. Samples were analysed after 7 days, 14 days and 35 days. After each immersion time, samples were removed from the solution and gently washed with distillate water. After drying under vacuum for several days at room temperature, films were weighted to monitor the weight loss.

Cellular proliferation. Cellular assays were performed using Vero and Cos-1 cells, from monkey kidney.

4500 mg of glucose/L and supplemented with 10% fetal bovine serum (FBS), penicillin (100 units/mL), and streptomycin (100 µg/mL). The cultures were maintained in a humidified incubator with an atmosphere of 5% CO_2 and 95% O_2 at 37ºC. Culture media were changed every two days. When cells reached 80-90% confluence, they were detached using 1-2 mL of trypsin (0.25% trypsin/EDTA) for 5 min at 37 °C. Finally, cells were re-suspended in 5 mL of

fresh medium and their concentration was determined with a Neubauer camera using 0.4% trypan blue.

PHMeEDOT and PTh-*g*-PCL deposited onto steel AISI 316 sheets of 0.5 0.5 cm^2 were placed in plates of 24 wells and sterilized using UV irradiation for 15 min in a laminar flux cabinet. An aliquot of 50 L containing 2 10^4 cells was deposited on the film surface at each well. Bare steel sheets were used as controls. Attachment of the cells was promoted by incubation under culture conditions for 30 min. Finally, 1 mL of the culture medium was added to each well. In order to evaluate cell viability after 120 h, colorimetric MTT [3-(4,5-dimethylthiazol-2-yl)-2,5-diphenyltetrazolium bromide] assays were conducted. Specifically, 50

samples were washed twice with PBS and stored in clean wells. In order to dissolve formed formazan crystals, 0.5 mL of DMSO/methanol/water (70/20/10 % v/v) was added. Finally, the

results derived from the average of five replicates (n= 5) for each independent experiment, were normalized to bare steel (control) as relative percentages.

RESULTS AND DISCUSSION

Synthesis and characterization of macromonomer

The oligo- -caprolactone based macromonomer, hereafter denoted Th-PCL, was prepared by ring opening polymerization (ROP) of -CL using Th-MeOH as initiator and stannous octanoate, $Sn(Oct)_2$, as catalyst (Scheme 2), following a slightly modified reported procedure.[55,56] In brief, appropriate amounts of -CL, initiator and catalyst (Table S1) were added under nitrogen in a previously flamed and nitrogen-purged two neck round-bottom flask equipped with a dropping funnel and magnetic stirrer. The -CL polymerization was carried out in bulk at 110 $^{\circ}$C. After 24 h, the mixture was diluted with CH_2Cl_2 and poured into a tenfold

excess of cold methanol. The polymer was collected after filtration and dried at room temperature in vacuum for 3 days.

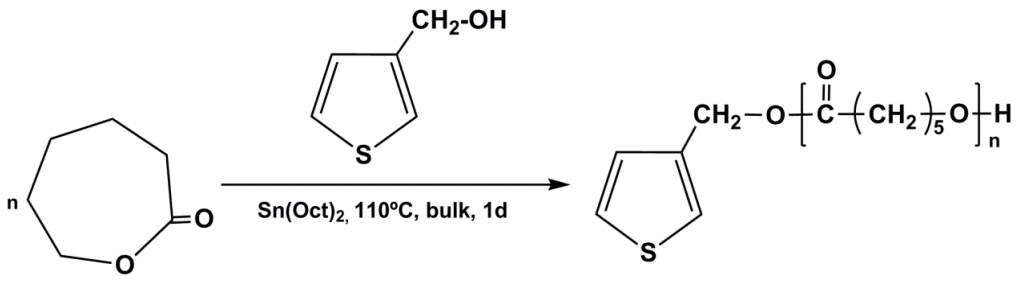

Scheme 2: Synthesis of the Th-PCL macromonomer

Th-PCL experimental number average molecular weight (M_n) was determined by using Eq. 2, with the integral values of the characteristic peaks from ^{1}H-NMR (Figure 1a), while that theoretically expected was calculated by using molar concentrations of reactant and initiator in the feed (Eq.3).

$$M_{n,NMR} \quad \frac{(I_{4.067} \quad I_{3.64})}{I_{5.12}} \; M_{n,\ CL} \quad M_{n,Th\ MeOH} \qquad (2)$$

$$M_{n,theor} \quad \frac{[\varepsilon \quad CL]}{[Th \quad MeOH]} \; M_{n,\ CL} \quad M_{n,Th\ MeOH} \qquad (3)$$

where $I_{4.067}$, $I_{3.64}$ and $I_{5.12}$ are the intensities of the peaks at 4.067 ppm, 3.64 ppm and 5.12 ppm, respectively, $M_{n,\ -CL}$ is the molecular weight of -CL (114.15 g/mol), $M_{n,Th\text{-}MeOH}$ is the molecular weight of Th-MeOH (114.16 g/mol), and a -CL: Th-MeOH molar ratio of 20:1.

There resulting values, $M_{n,NMR}$= 2511 g/mol and $M_{n,theor}$= 2430 g/mol, exhibit a very good agreement and are consistent with a polymerization degree of oligo- -caprolactone of n 21. The slight inaccuracy of M_n value, obtained by GPC measurements (see Supporting Information for details) is most probable due to the differences between the molecular characteristics of the polystyrene used as standards and the more polar oligo- -caprolactone, as observed in other cases.[55]

The FTIR spectrum of Th-PCL (Figure S1) presents strong absorptions originating from both the PCL chain and the thienyl ring: 3441cm^{-1} OH from oligo- -caprolactone chains ends; 3102

cm^{-1} (C H) stretching vibration and (C H) stretching vibration of the thienyl ring; 1726 cm^{-1} C=O ester from oligo- -caprolactone in crystalline form; 1557, 1540 cm^{-1} symmetric stretching vibrations of the thienyl ring; 1294 cm^{-1} (C O and C C) and 1189 cm^{-1}(O=C O) PCL crystallization-sensitive bands; 706 cm^{-1} C S; 581 cm^{-1} ring deformation; and 450 cm^{-1} C S C thienyl ring deformation.

The thermal behaviour of the synthesized macromonomer was investigated by DSC (Figure 1b). The calorimetric plot evidences an exothermic peak due to the crystallization of oligo- -caprolactone, which has a maximum at T_c= 31 ºC, and their melt at T_m= 55 ºC, these values being fully consistent with those reported in the literature for the pristine polymer.[67] On the other hand, the crystallinity found for the macromonomer was very high, $_c$= 0.66, which is fully consistent with the fact that the degree of crystallinity of PCL largely increases with decreasing molecular weight.[68]

Synthesis and characterization of PTh-g-PCL copolymers

Electropolymerization of Th-PCL macromonomer was unsuccessful, most probable due to the characteristics of its structure. The oligo- -caprolactone contains in its structural units electron-withdrawing ester groups, while the chain end shows a reactive hydroxyl function. As it was previously noticed,[69] such structural peculiarities could hinder electrochemical polymerization by a high oxidation potential. The ester group is a well-known moiety for increasing of oxidation potential.[70] Moreover, in some cases, the anodic polymerization of thiophenes with reactive functional groups (*e.g.* -NH_2, -OH and COOH) has been reported to be difficult due to their substantial nucleophilicity, which allow the functional groups to attack on the radical cation intermediates formed during electropolymerization, hence inhibiting the polymerization process.[71] On the other hand, tacking in account that the acetonitrile is a bad/non-solvent for polycaprolactone,[72] is very probable that it exists in the polymerization systems in a collapsed form, which sterically could hinder the reactive positions of the Th ring.

The incorporation of co-monomers is expected to reduce rapidly the grafting density, as was observed for PTh-*g*-PEG[39] and PTh-*g*-PEO[73] (PEO= polyethyleneoxide). As our final aim was to produce biocompatible grafted copolymers able to detect DA efficiently, HMeEDOT was selected as the most appropriated co-monomer for the preparation of PTh-*g*-PCL (Scheme 3).

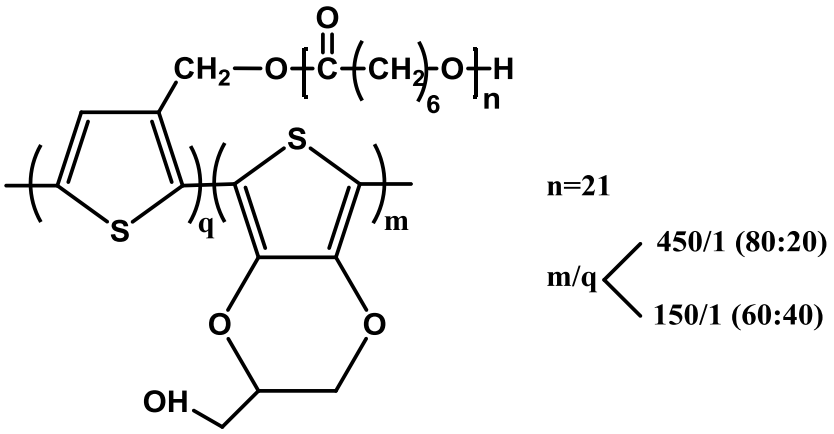

Scheme 3: Chemical structure of PTh-*g*-PCL

PTh-*g*-PCL films were prepared by CA using 80:20 and 60:40 HMeEDOT:Th-PCL molar ratios, while PHMeEDOT films were obtained as control. Investigation by CV of HMeEDOT and Th-PCL solutions in acetonitrile with 0.1 M TBATFB as supporting electrolyte (Figure S2), enabled us to choose the polymerization potential of +1.50 V, so that to maximizes the rate of the polymerization process without oxidizing the reaction medium, concomitantly avoiding the overoxidation of the generated materials. The polymerization time was also enlarged from = 500 s for 80:20 PTh-*g*-PCL and PHMeEDOT to = 800 s for 60:40 PTh-*g*-PCL due to the difficulties in the polymerization of Th-PCL macromonomer (*vide supra*). The average thickness (10 samples) of the films generated onto was 27.3 0.3, 31.1 0.5 and 26.7 0.4 m for 80:20 PTh-*g*-PCL, 60:40 PTh-*g*-PCL and PHMeEDOT, respectively, increasing to 29.0 1.5, 34.1 2.8 and 30.3 0.1 m when the substrate was ITO.

Figure 2a, which compares the FTIR spectra recorded for the HMeEDOT monomer and the prepared homopolymer, confirms the success of the anodic polymerization process. The monomer shows remarkable bands centered at 3099 and 752 cm^{-1}, which correspond to the C H stretching and out of plane mode, respectively. The absence of these two absorption bands in the PHMeEDOT spectrum indicates that the hydrogen atoms at the C -position are removed during the polymerization process. Other relevant bands in the PHMeDOT spectrum are observed at: 3450 $cm^{)}$ (O H stret.), 2923 and 2850 $cm^{)}$ (C H aliphatic stret.); 1466 and 1413 $cm^{)}$ (stret. modes of the thiophene ring); and 1060 $cm^{)}$ (C O stret.). The absorption bands in the FTIR spectra of the two copolymers (Figure 2b) confirm the incorporation of the Th-PCL (Figure 2b inset) to the polymer chain. Thus, the presence of oligo- -caprolactone grafted chains is reflected by the bands at 1726 cm^{-1} (C=O ester) and 1047 cm^{-1} (C O), the latter becoming broader and more intense than in the macromonomer because of the coexistence of both ester (from oligo- -caprolactone) and ether (from the dioxane ring of HMeEDOT) groups. On the other hand, the O H band at 3441 cm^{-1} (from both HMeDOT and PCL chain ends) and other peaks associated to the thiophene ring are also clearly identified.

Although determination of the final composition of 80:20 and 60:40 PTh-*g*-PCL is a very difficult task because of the insolubility of the copolymers, differences in the intensities of the bands reflect that the amount of Th-PCL units in the latter is significantly higher than in the former. In order to obtain a rough estimation of the composition of the two prepared PTh-*g*-PCL copolymers, the ratios of the areas associated to the absorptions band at 1723 cm^{-1} (C=O ester) and 1633 cm^{-1} (C=C stretching vibration of the Th ring) were evaluated. Results indicate that the copolymers derived from 80:20 and 60:40 HMeEDOT:Th-PCL molar ratio present, respectively, 450 and 150 HMeEDOT units per Th-PCL unit.

SEM micrographs of PHMeEDOT and PTh-*g*-PCL homogeneously deposited onto steel electrodes are displayed in Figure 3. The granular surface morphology of PHMeEDOT, which resembles that of PEDOT,[74] is affected by the incorporation of Th-PCL. However, a given

amount of macromonomer is required for such change. Thus, the structure of 80:20 PTh-*g*-PCL is similar to that observed for PHMeEDOT, while the amount of granules decreases for the 60:40 PTh-*g*-PCL. In any case, it should be highlighted that no phase separation or cracking was observed in films of the two copolymers.

Figure 4a compares de UV-vis spectra of PHMeEDOT and PTh-*g*-PCL copolymers. All spectra display a broad adsorption tail that starts at 480 nm, which is ascribed to the polaronic band of the conductive quinoid form.[75] As expected, the slope of such tail is more pronounced for the homopolymer than for the copolymers. Thus, the doping level of the copolymer chains decreases with the increasing amount of Th-PCL units. This doping level reduction could be due to the bulkiness of the Th-PCL units that can affect the overall planarity and rigidity of the copolymer chains. More specifically, planarity and rigidity of PHMeEDOT chains are mainly due to the restrictions imposed by the fused dioxane ring and to the electron-donating effects provided by the oxygen atoms contained in such cyclic substituents.[76] By considering these experimental results, it seems that the incorporation of Th-PCL units locally perturbs the planarity of copolymers chains, producing a loss in aromaticity, and this adverse effect increased with the increasing number of Th-PCL units into the copolymers chains.

Control voltammograms of PHMeEDOT and PTh-*g*-PCL deposited onto steel sheets in PBS 0.1 M (Figure 4b) indicates that the anodic peak detected at +0.15 V in the homopolymer, which has been attributed to the formation of polarons in the PTh chain, shifts to higher potentials in the copolymers. Moreover, the charge stored in homopolymer films is around 2-9% higher than in the copolymer ones, which is fully consistent with loss in aromaticity in the MeHEDOT-chains induced by the incorporation of macromonomer units. Voltammograms registered after 25 consecutive oxidation-reductions cycles are included in Figure 4b. As it can be seen, the electrochemical activity decreases in all cases, especially for 60:40 PTh-*g*-PCL copolymer. Specifically, the LEA obtained for PHMeEDOT, 80:20 PTh-*g*-PCL and 60:40 PTh-*g*-PCL was 19%, 21% and 30%, respectively.

The homopolymer and copolymers were also deposited onto GC, which is the substrate typically used for the electrochemical detection of DA using PEDOT.[32,35] The shape of the registered control voltammograms (Figure 4c) was similar to those recorded for the materials deposited onto steel. However, the amount of charge reversibly exchanged in 0.1 M PBS was significantly lower for the materials deposited onto GC than for those obtained using steel electrodes. Thus, the electroactivity of PHMeEDOT polymerized onto GC was 86% lower than that of the homopolymer deposited onto steel, the differences determined for 80:20 and 60:40 PTh-*g*-PCL being of 56% and 87%, respectively. In spite of this drawback, it is worth noting that the electroactivity of 80:20 PTh-*g*-PCL generated onto GC is 280% higher than that of PHMeEDOT prepared using same substrate. This behavior has been attributed to a combination of two features. On the one hand, the 80:20 copolymer deposited onto GC is more porous than PHMeEDOT, facilitating the access and escape of dopant ions during the oxidation and reduction processes, respectively. On the other hand, PCL chains tend to form separated phases when the 60:20 copolymer is generated onto GC, which obviously affects negatively to the electroactivity of the film. The latter drawback is not observed for 80:20 PTh-g-PCL. These two features are clearly illustrated in the SEM images displayed in Figure 4d.

Biodegradability, wettability, cytotoxicity and biocompatibily of PTh-g-PCL copolymers

After 35 days of immersion in PBS solution, PHMeEDOT and PTh-*g*-PCL films retained both the adherence and the mechanical integrity of the films (Figure S3). Although films showed some surface erosion, suggesting that water penetrates in the PCL domains of the copolymer chains, the weight loss (WL) was very small (*i.e.* WL= 0.5 and 1.3% for 80:20 and 60:40 PTh-*g*-PCL, respectively, in Figure S4). On the other hand, the contact angle ( ) determined for PHMeEDOT and PCL are < 10º and 86º 5º, indicating that the former is very hydrophilic while the latter is just at the boundary between hydrophilic and lipophilic. The values of the 80:20 and 60:40 PTh-*g*-PCL (37º 2º and 41º 1º, respectively) are intermediate between those of the

two homopolymers and increases with the content of Th-PCL. Considering that the RMS roughness (Rq) of PHMeEDOT, 80:20 PTh-*g*-PCL and 60:40 PTh-*g*-PCL are very similar (Rq= 5.1 1.0, 5.9 0.3 and 6.2 0.2 m, respectively), differences in the wettability of PHMeEDOT and the copolymer should be exclusively attributed to the chemistry of films surfaces, more specifically to the organization of oligo- -caprolactone chains. Although the content of Th-PCL is low in PTh-*g*-PCL, results suggest a biphasic organization similar to that reported for other grafted copolymers:[37] PTh and PCL segments are perpendicular and parallel to the surface, respectively. This explanation is also supported by the fact that acetonitrile is a bad solvent for oligo- -caprolactone chains and, during solvent evaporation, these moieties will be oriented to the film surface due to their natural tendency to exit from the solution earlier. This phenomenon could be enhanced by the formation of intra- and intermolecuar hydrogen bonds between oligo- -caprolactone chains, the hydroxylic chain ends and hydroxyl function of PHMeEDOT. Thus, oligo- -caprolactone chains expose their hydrophobic aliphatic parts towards the film surface. As acetonitrile is a enough high boiling point solvent, these phenomena are most likely to take place.

The effect of the grafted oligo- -caprolactone chains in cytotoxicity and biocompatibility of PTh backbone chains was evaluated by considering epithelial (Vero) and fibroblast (Cos-1) cell lines derived from monkey kidney. For this purpose, the potential cytotoxicity of the PHMeEDOT and PTh-*g*-PCL was elucidated by culturing cells in plate wells containing steel sheets covered by these organic materials. Cell cultures on bare steel plates were used as controls.

Cytotoxicity was determined after five days using the MTT assay and quantifying all viable cells contained in the wells, which allowed us to consider the toxic effects associated not only to the polymeric matrix but also to small molecules (*e.g.* acetonitrile, monomer, macromonomer and dopant molecules) or oligomers that could be eventually released to the medium. Results displayed in Figure 5a reflect the cytotoxic effects of PHMeEDOT, which reduce cells viability

about 20-

100 μM UA in 0.1 M PBS are displayed in Figures 6a and 6b for the steel- and GC-modified electrodes, respectively. As it can be seen, the oxidation peaks of DA, AA and UA are much better defined for the electrodes deposited on GC than on steel, this feature being especially noticeable for the 80:20 PTh-*g*-PCL copolymer (Figure 6b). Furthermore, the oxidation peak potential of DA at the latter copolymer is clearly identified at 0.34 V, whereas the peak potential of oxidation of AA corresponds to -0.01 V and the one for UA exceeds the reversal potential. Accordingly, both the separation among the peak potentials and the high strength of the current signal for the oxidation of DA suggest that 80:20 PTh-*g*-PCL is an appropriated sensor for the latter neurotransmitter in terms of both resolution and sensitivity.

Figure 6c shows cyclic voltammograms of solution mixtures with different DA concentration (from 50 to 0.5 M), 200 μM AA and 100 μM UA in 0.1 M PBS for the 80:20 PTh-*g*-PCL sensor. The grafted copolymer is able to catalyse the oxidation of DA molecules in a low potential range, which means that in cellular systems, the voltage applied would be the minimal to detect this kind of biomolecule *in vivo*. The anodic peak current decreases with the decreasing concentration of DA, while the peak potential remains almost constant at 0.34-0.35 V for all concentrations. Even if the response of DA is very week for concentrations below 0.5 M, however this threshold is around the one that would be desirable (*i.e.* the synaptic DA concentration is 1.6 mM).

The calibration curve (Figure 6d) shows a good rectilinear behaviour for low concentrations only (5 M). The correlation coefficient for the first oxidation-reduction cycle is 0.9985, while the anodic peak currents determined for 0.5 and 5 M DA are 128.2 and 270.0 A, respectively. It is worth noting that both the linearity of the profile and sensitivity obtained for 80:20 PTh-*g*-PCL are higher than those obtained for PHMeEDOT (Figure 6e). The calibration curve obtained for the latter provides a correlation coefficient of 0.9349 only, while the anodic peak currents measured for 0.5 and 5 M DA were 13.6 and 29.10 A, respectively. Unfortunately, the response exhibited by the 60:40 PTh-*g*-PCL copolymer was not consistent, as

is reflected in Figure 6f. Thus, the anodic peak current changed erratically when the DA concentration was increased or decreased.

CONCLUSIONS

In summary, Th-based graft copolymers, incorporating a few amounts of oligo- -caprolactone -containing electroactive macromonomer into PHMeEDOT chains, have been synthesized using the "*macromonomer technique*" *via* electrochemical polymerization. When comparing with PHMeEDOT homopolymer, the oligo- -caprolactone grafted chains onto copolymers main chains reduce considerably the cytotoxicity of the resulted films formed during polymerization on the electrode surface. Furthermore, the 80:20 PTh-*g*-PCL copolymer generated onto GC electrodes is more electroactive than PHMeEDOT since the former becomes more porous than the latter. As a consequence, sensing capability of 80:20 PTh-*g*-PCL for DA detection is demonstrated to be much higher, sensitive and selective than that of PHMeEDOT. Overall, the 80:20 PTh-g-PCL could considered as an alternative, potential candidate for the fabrication of implantable DA sensors.

ACKNOWLEDGEMENTS

This work was supported by MINECO (MAT2015-69367-R). Support for the research of the Generalitat de Catalunya. B.G.M. is thanked to CONACYT for the financial support through a postgraduate scholarship (328467 CVU 621314). The Romanian authors dedicate this paper to the memory of Professor Cristofor I. Simionescu, (1920-2007), a remarkable academic and cultural personality, the pioneer of macromolecular chemistry in Romania.

REFERENCES

1. R. L. DiMarco and S. C. Heilshorn, *Adv. Mater.*, 2012, **24**, 3923.

2. J. Huang and A. Heise, *Chem. Soc. Rev.*, 2013, **42**, 7373.

3. J. Wu, N. Kamly, J. Shi, L. Zhao, Z. Xiao, G. Hollett, R. John, S. Ray, X. Xu, X. Zhang, P. W. Kantoff and O. C. Farokhzad, *Angew. Chem., Int. Ed.*, 2014, **53**, 8975.

4. C. L. McGann, E. A. Levenson and K. L. Kiick, *Macromolecules*, 2013, **214**, 203.

5. R. Dong, X. Zhao, B. Guo and P. X. Ma, *ACS Appl. Mater. Interfaces*, 2016, **8**, 17138.

6. H. Schlaad, B. Smarsly and M. Losik, *Macromolecules*, 2004, **37**, 2210.

7. H. T. Nguyen, S. Sapp, C. Wei, J. K. Chow, A. Nguyen, J. Coursen, S. Luebben, E. Chang, R. Ross and C. E. Schmidt, *J Biomed Mater Res Part A* , 2014, **102A**, 2554.

8. A. G. Guex, C. D. Spicer, A. Armgarth, A. Gelmi, E. J. Humphrey, C. M. Terraciano, S. E. Hardy and M. M. Stevens, *MRS Commun.*, 2017, DOI:10.1557/mrc.2017.45

9. M. Müllner, *Macromol. Chem. Phys.*, 2016, **217**, 2209.

10. F. Qiu, Y. Huang and X. Zhu, *Macromol. Chem. Phys.*, 2016, **217**, 266.

11. I. V. Dimitrov, I. V. Berlinova and N. G. Vladimirov, *Macromolecules*, 2006, **39**, 2423.

12. P. Anbinder, C. Macchi, J. Amalvy and A. Somoza, *Carbohydr. Polym.*, 2016, **145**, 86.

13. J. Yang, K. Wu, C. Konak and J. Kopecek, *Biomacromolecules*, 2008, **9**, 510.

14. B. Kuei and E. D. Gomez, *Soft Matter*, 2017, **13**, 49.

15. G. Wegner, *Macromol. Chem. Phys.*, 2003, **204**, 347.

16. A.D. Bendrea, L. Cianga, and I. Cianga, *J. Biomater. Appl.*, 2011, **26**, 3.

17. G. Baolin, L. Glavas and A.-C. Albertsson, *Prog. Polym. Sci.*, 2013, **38**, 1263.

18. T. Darmanin and F. Guittard, *Prog. Polym. Sci.*, 2014, **39**, 656.

19. J. Heinze, B. A. Frontana-Uribe and S. Ludwigs, *Chem. Rev.*, 2010, **110**, 4724.

20. A. Guiseppi-Elie, *Biomaterials*, 2010, **31**, 2701.

21. T. F. Otero, J. G. Martínez and J. Arias-Pardilla, *Electrochim. Acta*, 2012, **84**, 112.

22. M. M. Pérez-Madrigal, E. Armelin, J. Puiggalí and C. Alemán, *J. Mater. Chem. B*, 2015, **3**, 5904.

23. R. Green and M. R. Abidian, *Adv. Mater.*, 2015, **27**, 7620.

24. Z. H. Wang, P. Tammela, J. X. Huo, P. Zhang, M. Stromme and L. Nyholm, *J. Mater. Chem. A*, 2016, **4**, 1714.

25. D. E: López-Pérez, D. Aradilla, L. J. del Valle and C. Alemán, *J. Phys. Chem. C*, 2013, **117**, 6607.

26. U. Lauter, W. H. Meyer and G. Wegner, *Macromolecules*, 1997, **30**, 2092.

27. N. Hadjichristidis, M. Pitsikalis, H. Iatrou and S. Pispas, *Macromol. Rapid Commun.*, 2003, **24**, 979.

28. M. Müllner and A. H. E. Müller, *Polymer*, 2016, **98**, 389.

29. D.G. Colak, I. Cianga, L. Cianga and Y. Yagci, *Des. Monom. Polym.*, 2016,

39. S. Maione, G. Fabregat, L. J. del Valle, A.-D. Bendrea, L. Cianga, I. Cianga, F. Estrany and C. Alemán, *J. Polym. Sci., Part B: Polym. Phys.*, 2015, **53**, 239.

40. Y. Kim, H. J. Kim, J-S. Kim, R. C. Hayward and B. J. Kim, *ACS Appl. Mater. Interfaces*, 2017, **9**, 2933.

41. E. Sahin, P. Camurlu, L. Toppare, V. M. Mercore, I. Cianga and Y. Yagci, *J. Electroanal. Chem.*, 2005, **579**, 189.

42. J. Shen, H. Masaoka, K. Tsuchiya and K. Ogino, *Polym. J.*, 2008, **40**, 421.

43. D. Ag, M. Seleci, R. Bongartz, M. Can, S. Yurteri, I. Cianga, F. Stahl, S. Timur, T. Scheper and Y. Yagci, *Biomacromolecules*, 2013, **14**, 3532.

44. C. Yang, H. Liu, Y. Zhang, Z. Xu, X. Wang, B. Cao and M. Wang, *Biomacromolecules*, 2016, **17**, 1673.

45. H. Akbulut, M. Yavuz, E. Guler, D. Odaci Demirkol, T. Endo, S. Yamada, S. Timur and Y. Yagci, *Polym. Chem.*, 2014, **5**, 3929.

46. B. Demir, T. Yilmaz, E. Guler, Z. Pinar Gumus, H. Akbulut, E. Aldemir, H. Coskunol, D. Goen Colak, I. Cianga, S. Yamada, S. Timur, T. Endo and Y. Yagci, *Talanta*, 2016, **161**, 789.

47. Y. Z. Long, M. M. Li, C. Z. Gu, M. X. Wan, J. L. Duvail, Z. W. Liu and Z. Y. Fan, *Prog. Polym. Sci.*, 2011, **36**, 1415.

48. S. Kirchmeyer and K. Reuter, *J. Mater. Chem.*, 2005, **15**, 2077.

49. G. Fabregat, F. Estrany, M. T. Casas, C. Alemán and E. Armelin, *J. Phys. Chem. B*, 2014, **118**, 4702.

50. N.F. Atta, A. Galal and R.A. Ahmed, *Bioelectrochemistry*, 2011, **80**, 132.

51. E. R. Kandel, J. H. Schwartz and T. M. Jessel, Principles of Neural Science, fourth ed., McGraw-Hill, New York, 2000, pp. 207 298.

52. G. Fabregat, J. Casanovas, E. Redondo, E. Armelin and C. Alemán, *Phys. Chem. Chem. Phys.*, 2014, **16**, 7850.

53. C. Jerome, L. Martinot, P. Louette and R. Jerome, *Macromol. Symp.*, 2000, **153**, 305.

54. Y. Wang, B. Erdogan, J. N. Wilson and U. H. F. Bunz, *Chem. Commun.*, 2003, 1624.

55. S. Yurteri, I. Cianga, M. Degirmenci and Y.Yagci, *Polym Int.*, 2004, **53**, 1219.

56. I. Kerman , L. Toppare , F. Yilmaz and Y. Yagci, *J. Macro. Sci., Part A*, 2005, **42**, 509.

57. A.-D. Bendrea, L. Vacareanu and M. Grigoras, *Polym. Int.*, 2010, **59**, 624.

58. A. L. Demirel, S. Yurteri, I. Cianga and Y. Yagci, *Macromolecules*, 2005, **38**, 6402.

59. A. L. Demirel, S. Yurteri, I. Cianga and Y. Yagci, *J. Polym. Sci. Part A: Polym. Chem.*, 2007, **45** 2091.

60. J. N. Wilson, Y. Wang, J. J. Lavigne and U. H. F. Bunz, *Chem. Commun.*, 2003, 1626.

61. B. Kulkarni, B. Surnar and M. Jayakannan, *Biomacromolecules*, 2016, **17**, 1004.

62. X. Li, S. L. Prukop, S. L. Biswal and R. Verduzco, *Macromolecules*, 2012, **45**, 7118.

63. R. Barbey, L. Lavanant, D. Paripovic, N. Schüwer, C. Sugnaux, S. Tugulu and H.-A. Klok, *Chem. Rev.*, 2009, **109**, 5437.

64. L. T. Strover, J. Malmström, L. A. Stubbing, M. A. Brimble and J. Travas-Sejdic, *Electrochim. Acta*, 2016, **188**, 57.

65. J.P. Mofokeng and A.S. Luyt, *J. Mater. Sci.*, 2015, **50**, 3812.

66. V. Crescenzi, G. Manzini, G. Calzolari and C. Borri, *Eur. Polym. J.*, 1972, **8**, 44.

67. L. G. M. Beekmans and G. J. Vancso, *Polymer*, 2000, **41**, 8975.

68. M. J. Jenkins and K. L. Harrison, *Polym. Adv. Technol.*, 2006, **17**, 474.

69. M. M. Pérez-Madrigal, L. Cianga, L. J. del Valle, I. Cianga and C. Alemán, *Polym. Chem.*, 2015, **6**, 4319.

70. B. X. Valderrama-García , E. Rodríguez-Alba , E. G. Morales-Espinoza, K. Moineau Chane-Ching and E. Rivera, *Molecules*, 2016, **21**, 172.

71. G. Li, G. Koßmehl, H.- P. Welzel, G. Engelmann, W.- D. Hunnius, W. Plieth and H. Zhu, *Macromol. Chem. Phys.*, 1998, **199**, 525.

72. C. J. Luo, E. Stride and M. Edirisinghe, *Macromolecules*, 2012, **45**, 4669.

73. L. Qi, M. Sun and S. Dong, *J. Appl. Polym. Sci.*, 2006, **102**, 1803.

74. S. Maione, A. M. Gil, G. Fabregat, L. J. del Valle, J. Triguero, A. Laurent, D. Jacquemin, F. Estrany, A. I. Jiménez, D. Zanuy, C. Cativiela and C. Alemán, *Biomater. Sci.*, 2015, **3**, 1395.

75. S. Garreau, G. Louarn, J. P. Buisson, G. Froyer and S. Lefrant, *Macromolecules*, 1999, **32**, 6807.

76. J. Poater, J. Casanovas, M. Solà and C. Alemán, *J. Phys. Chem. A*, 2010, **114**, 1023.

CAPTIONS TO FIGURES

Figure 1. (a) ^{1}H-NMR spectrum of Th-PCL macromonomer in $CDCl_3$. (b) DSC traces of Th-PCL macromonomer.

Figure 2. FTIR spectra of (a) PHMeEDOT and (b) 80:20 and 60:40 PTh-*g*-PCL copolymers, synthesized used steel as working electrode. The spectrum of Th-PCL macromonomer has been included as inset.

Figure 3. Low (left side) and high (right side) resolution SEM micrographs of (a,b) PHMeEDOT, (b) 80:20 PTh-*g*-PCL and (c) 60:40 PTh-*g*-PCL films deposited onto steel as working electrode

Figure 4. (a) UV-vis spectrum of PHMeEDOT, 80:20 PTh-*g*-PCL and 60:40 PTh-*g*-PCL deposited onto ITO. The spectra are normalized according the thickness of the film. First control voltammogram (solid lines) and voltammogram after 25 consecutive oxidation-reduction cycles (dashed lines) in PBS 0.1 M for PHMeEDOT, 80:20 PTh-*g*-PCL and 60:40 PTh-*g*-PCL deposited onto (b) stainless steel and (c) GC. (d) SEM images of PHMeEDOT, 80:20 PTh-*g*-PCL and 60:40 PTh-*g*-PCL deposited onto GC.

Figure 5. (a) Cytotoxycity and (b) biocompatibility of f PHMeEDOT, 80:20 PTh-*g*-PCL and 60:40 PTh-*g*-PCL deposited onto steel (five samples for each group). Bars represent the mean standard deviation. The relative viability of Vero and Cos-1 cells was established in relation to bare steel, which was considered as control substrate.

Figure 6. Cyclic voltammograms at electrodes consisting of PHMeEDOT and PTh-*g*-PCL deposited onto (a) steel and (b) GC in 0.1 M PBS with 100 M DA, 200 M AA and 200 M UA. (c) Comparison of DA detection intensity from 0.5 to 50 M in 0.1 M PBS with 200 M AA and 200 M UA. All voltammograms were obtained by scanning from -0.40 to 0.80 V at a scan rate of 50 mV/s. Calibration curves for DA detection in the concentration range from 0.5 to 5 M (to 50 M in inset) in 0.1 M PBS with 200 M AA and 200 M UA for (d) 80:20 PTh-*g*-PCL, (e) PHMeEDOT, and (f) 60:40 PTh-*g*-PCL deposited onto GC.

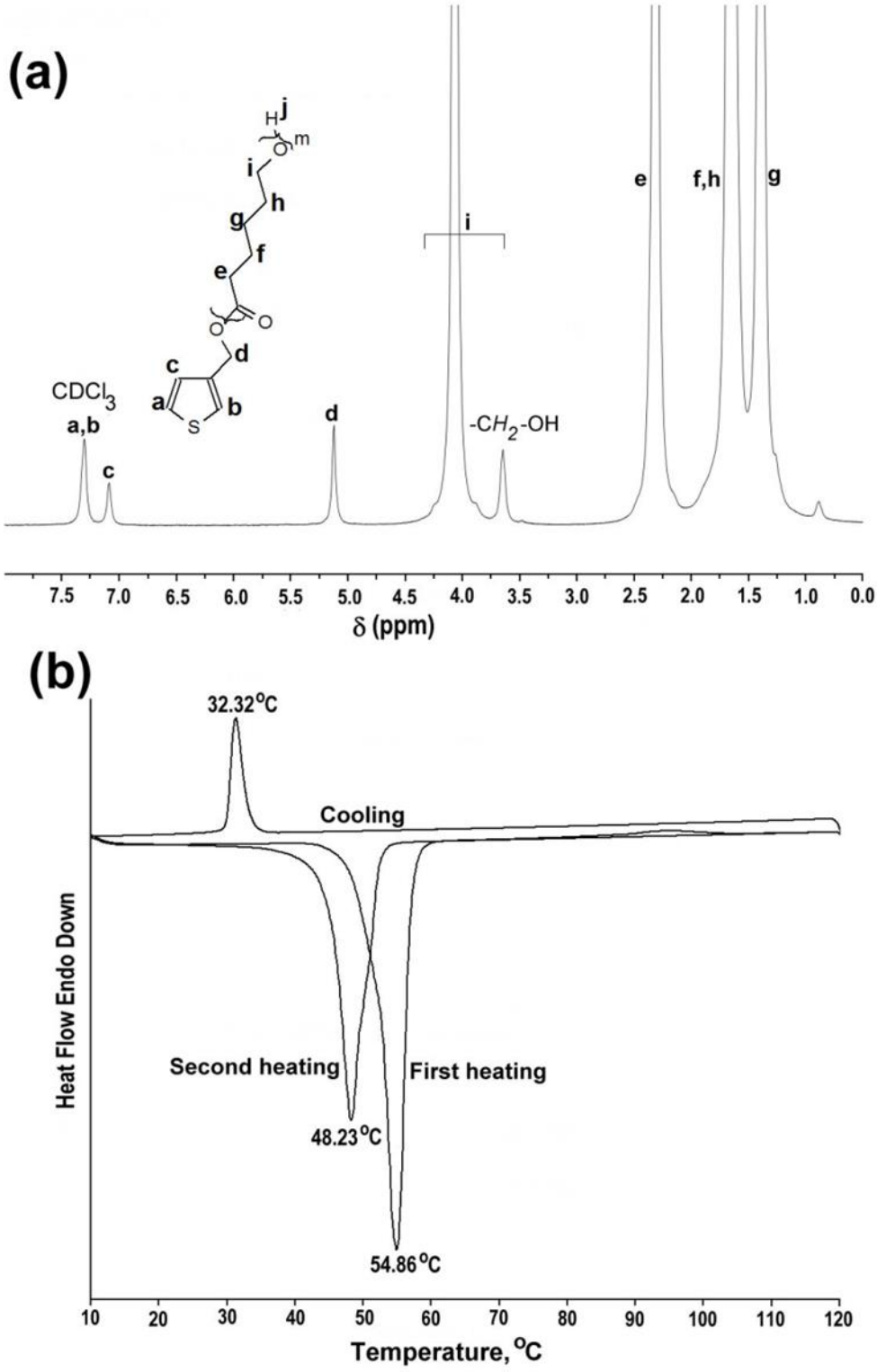
(a)
CDCl3
a,b
c
d
-CH2-OH
e
f,h
g
i
δ (ppm)
(b)
32.32°C
Cooling
Heat Flow Endo Down
Second heating
First heating
48.23°C
54.86°C
Temperature, °C

Figure 1

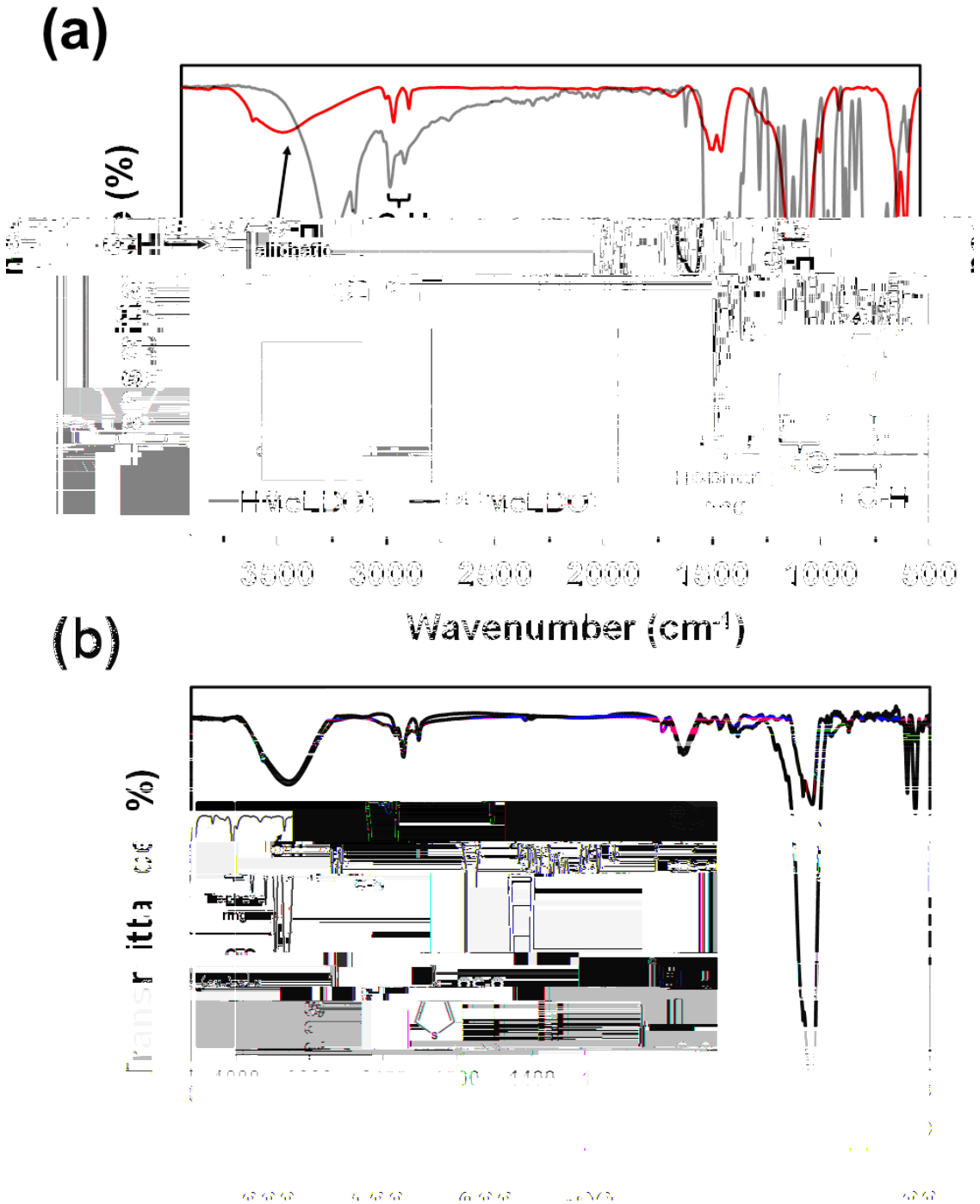

Figure 2

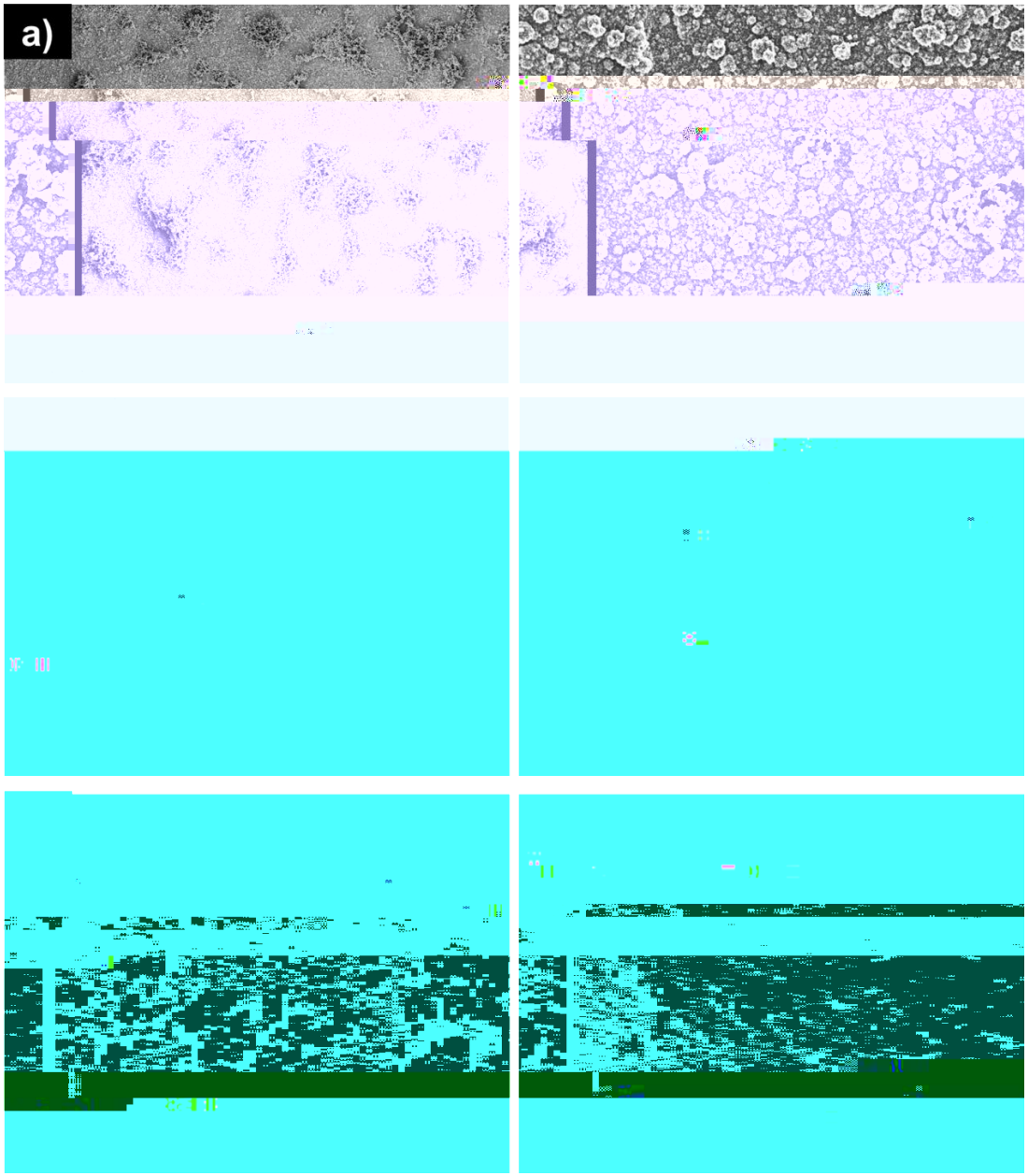

Figure 3

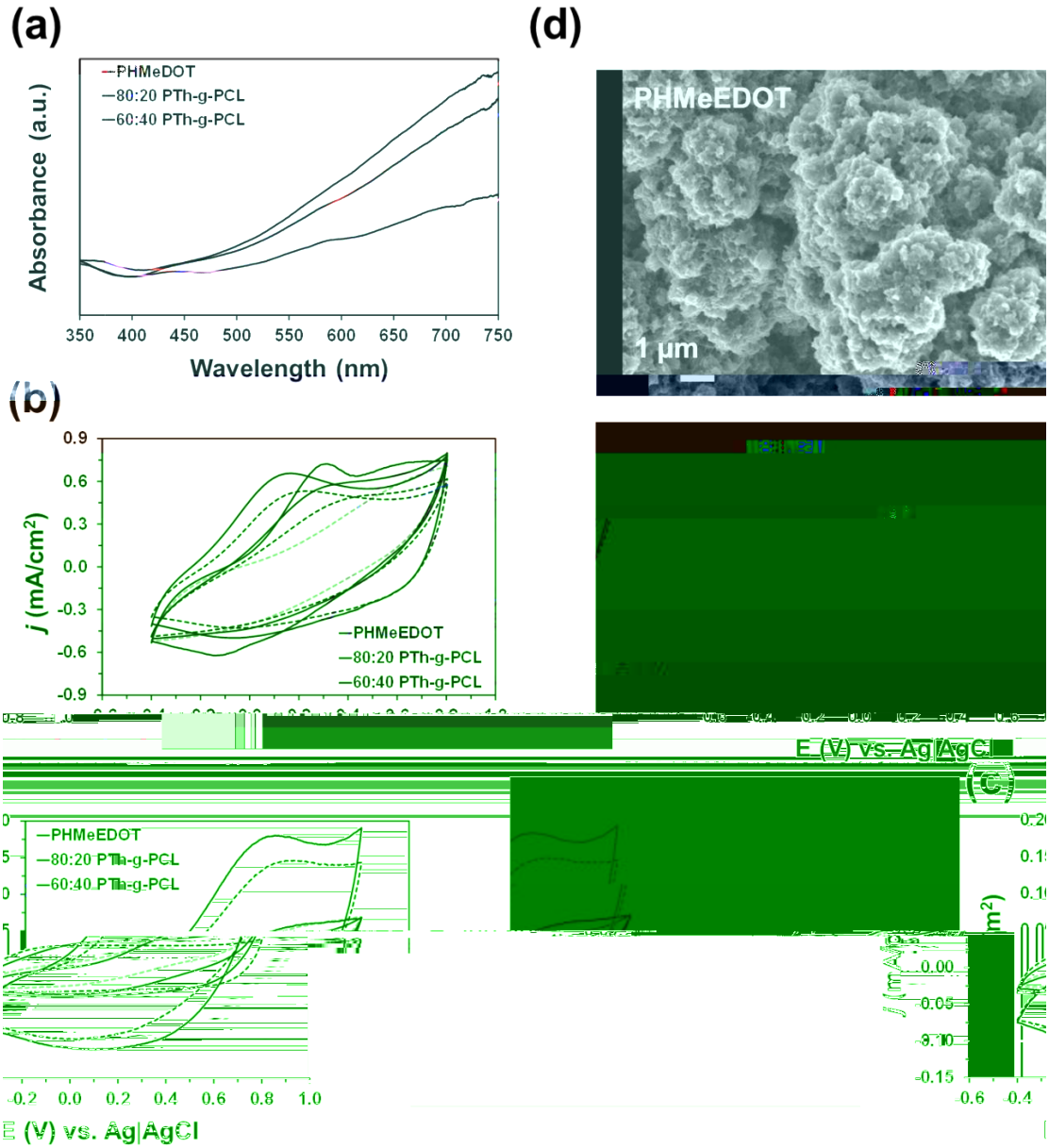
(a)
PHMeDOT
80:20 PTh-g-PCL
60:40 PTh-g-PCL
Absorbance (a.u.)
350 400 450 500 550 600 650 700 750
Wavelength (nm)
(d)
PHMeEDOT
1 µm
(b)
0.9 0.6 0.3 0.0 -0.3 -0.6 -0.9
j (mA/cm²)
PHMeEDOT
80:20 PTh-g-PCL
60:40 PTh-g-PCL
E (V) vs. Ag|AgCl
(c)
PHMeEDOT
80:20 PTh-g-PCL
60:40 PTh-g-PCL
-0.2 0.0 0.2 0.4 0.6 0.8 1.0
E (V) vs. Ag|AgCl
0.00
-0.05
-0.10
-0.15
-0.6 -0.4

Figure 4

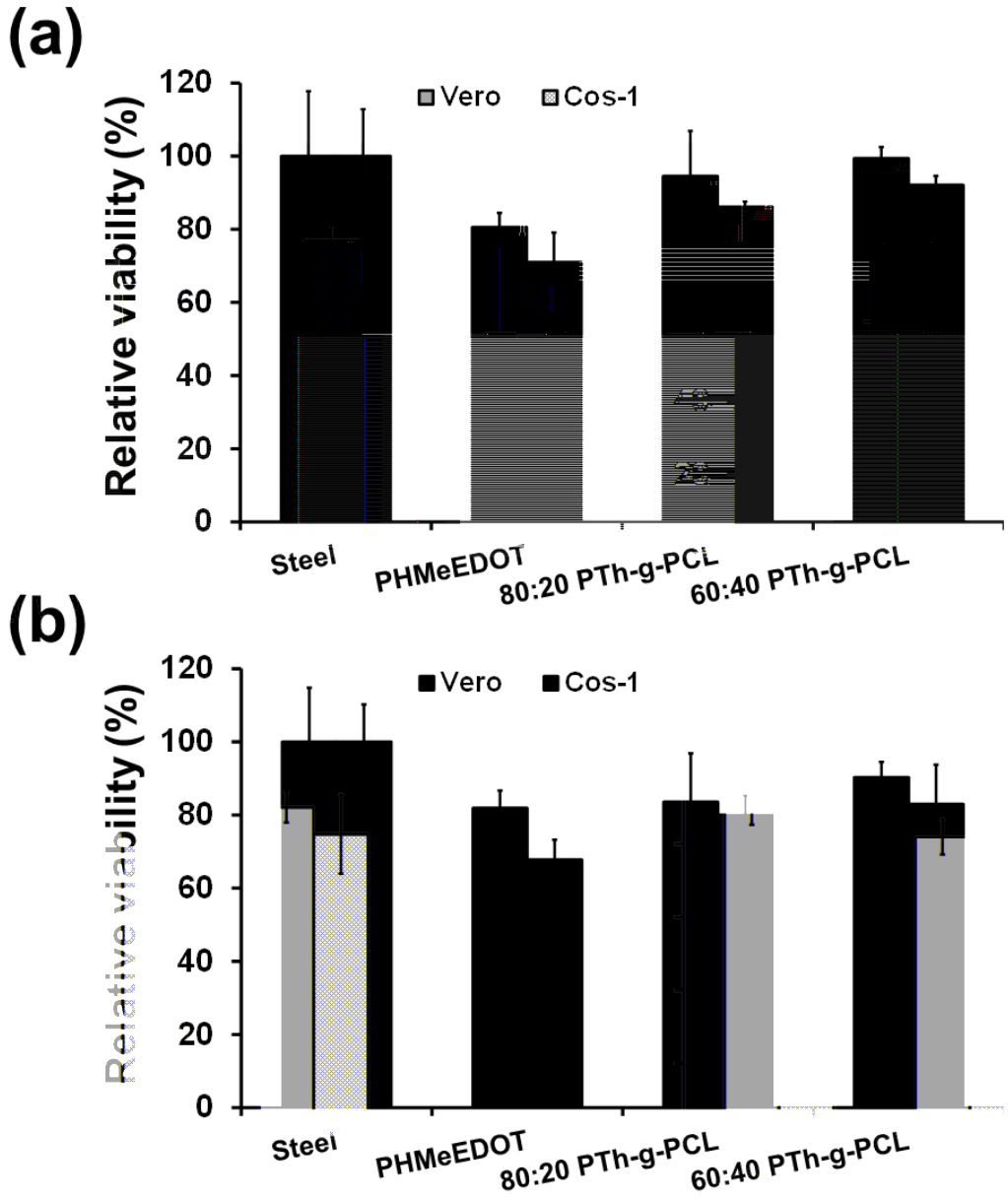
(a)
Relative viability (%)
120
100
80
60
40
20
0
Vero
Cos-1
Steel
PHMeEDOT
80:20 PTh-g-PCL
60:40 PTh-g-PCL
(b)
Relative viability (%)
120
100
80
60
40
20
0
Vero
Cos-1
Steel
PHMeEDOT
80:20 PTh-g-PCL
60:40 PTh-g-PCL

Figure 5

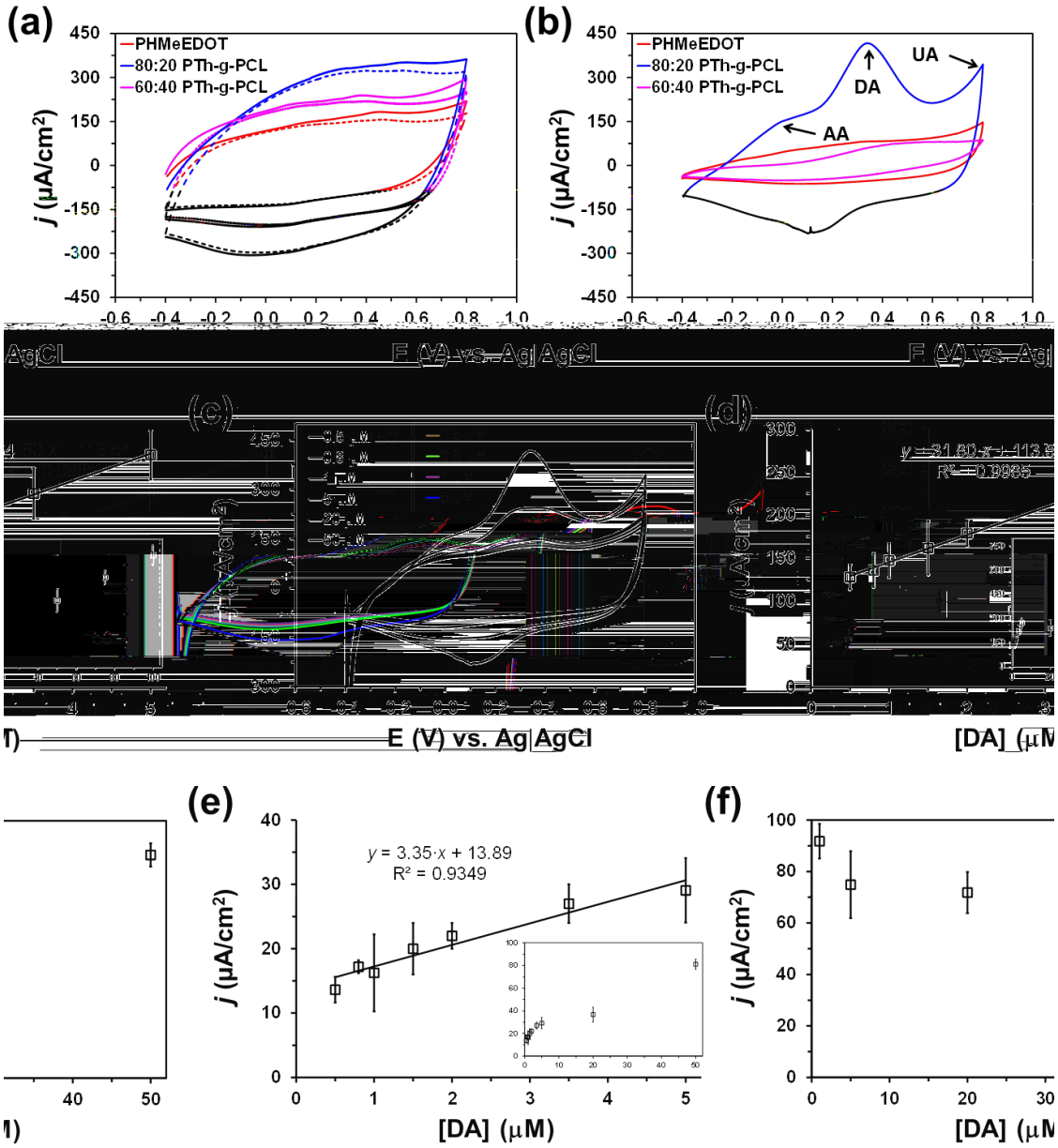
(a)
PHMeEDOT
80:20 PTh-g-PCL
60:40 PTh-g-PCL
j (μA/cm²)
(b)
PHMeEDOT
80:20 PTh-g-PCL
60:40 PTh-g-PCL
UA
DA
AA
j (μA/cm²)
E (V) vs. Ag|AgCl
(c)
(d)
E (V) vs. Ag|AgCl
[DA] (μM)
(e)
y = 3.35·x + 13.89
R² = 0.9349
j (μA/cm²)
[DA] (μM)
(f)
j (μA/cm²)
[DA] (μM)

Figure 6

Graphical Abstract